MATERIALS
SCIENCE

Determination of residual stresses and material properties by an energy-based method using artificial neural networks

Hongping Jin, Wenyu Yang[*], and Lin Yan

The State Key Lab of Digital Manufacturing Equipment and Technology, Mechanical Science and Engineering, Huazhong University of Science and Technology, Wuhan 430074, China

Abstract. With the help of an energy-based method and dimensional analysis, an artificial neural network model is constructed to extract the residual stress and material properties using spherical indentation. The relationships between the work of residual stress, the residual stress, and material properties are numerically calibrated through training and validation of the artificial neural network (ANN) model. They enable the direct mapping of the characteristics of the indentation parameters to the equi-biaxial uniform residual stress and the elastic–plastic material properties. The proposed ANN can quickly and effectively predict the residual stress and material properties based on the load–depth curve of spherical indentation.

Key words: spherical indentation, residual stress, material properties, finite element analysis.

1. INTRODUCTION

Determining the residual stress is crucial in a wide variety of systems because residual stress in materials and structures is associated with fatigue, corrosion, wear, and failures of the systems. The traditional methods of measuring residual stress can be divided into two categories: destructive and non-destructive methods. Destructive methods, including hole-drilling and saw-cutting techniques, etc., can generally be used to measure residual stress quantitatively without any reference sample, but they have destructive characteristics. Non-destructive methods, including X-ray and neutron diffraction, etc., can measure the residual stress without destruction. However, they are generally expensive and complex. Moreover, they are highly sensitive to such metallurgical factors as grain size and texture [1].

Instrumented indentation has been used to measure the mechanical properties of materials [2–7], such as hardness H, elastic modulus E, strain-hardening expo-

nent n, and yield strength σ_y. During indentation, a rigid indenter is penetrated normally into a homogeneous solid while the indentation load F and depth h are continuously recorded during one complete cycle of loading and unloading. Because the indentation load–depth curve reflects the behaviour of the material under indentation loading and unloading, indentation can be used to evaluate material properties. However, finite element model (FEM) and experimental investigations have shown that residual stress has a significant effect on the load–depth curve. General observations reveal that tensile stress tends to stretch out the load–depth curves, a smaller force can push the indenter down to the same indentation depth, while compressive stress compresses the curves, and thus a larger load is required to achieve the same indentation depth [8]. This is the reason why indentation can also be used to evaluate the residual stress.

Several methodologies have been introduced to estimate residual stress using instrumented indentation. The earliest effort was to examine the relationship between hardness and residual stress. The results suggest that hardness measurement may be used to

characterize residual stress in materials [8,9]. However, the change in the hardness by the residual stress is less than 10% of its unstressed value, and the effects of compressive stress are often not as large as those of tensile stress. In addition, the effects of residual stress on the indentation profile are relatively large, e.g., the residual stress can change the state of pile-up or sink-in, which causes a large error in the area measurement, and these errors result in a larger error in the residual stress measurement because determination of the hardness requires measurement of the indentation area.

Suresh and Giannakopoulos [8] used the difference in the contact area of stressed and unstressed specimens indented to the same depth to determine the residual stress. Based on this method, Lee and Kwon [10] developed a new method to estimate residual stress by analysing the surface stress effect on contact pressure in terms of shear plasticity during depth-controlled indentation. Comparison with the results of conventional saw-cutting tests showed that the indentation test could be effectively and easily used for the assessment of residual stress. However, their methods for residual stress determination require an unstressed reference sample and the residual indentation area needs to be measured.

Chen et al. [11], Zhao et al. [12], and Yan et al. [13] proposed alternative methods to measure the residual stress and perfectly elastic–plastic properties by using dimensional analysis and reverse analysis for conical microindentation, respectively. Their methods do not require measurement of a contact radius and a reference stress-free material. However, the accuracy of such approaches is highly dependent on the precision of the curve or surface fitting procedure as well as the robustness of the reverse analysis algorithm.

Xu and Li [14] found that the ratio of elastic recovery displacement of nanoindentation to the maximum penetration depth has a linear relationship to the ratio of residual stress to yield stress. Therefore, they presented an empirical model for residual stress determination from the elastic recovery displacement of nanoindentation. However, for very soft materials, this ratio is basically independent of the residual stress. Thus, this model may be suitable for the determination of residual stress only in very hard materials.

Based on the premise that elastic unloading responses during indentation are fully independent of residual stress, Wang et al. [15] derived a formula for determining the residual stress using sharp indentation and the energy method. This model assumes that there is no variation in the indent angle after the removal of the load. However, it is known that the surface profile undergoes a large change during the unloading stage due to the elastic recovery of the material. For this reason, this assumption would overestimate the residual stress.

Dean et al. [16] found that the peak indentation load is fairly sensitive to the presence of residual stress and they used nanoindentation to measure residual stresses in surface layers. They pointed out that this technique is well suited for the mapping of residual stresses over the surface of a component because nanoindentation involves investigation of relatively small volumes of material. They also argued that using hardness as a measured parameter to determine residual stress will cause difficulties, since the sensitivity of hardness is lower and less consistent because the influence of pile-up on the area of contact is larger.

Swadener et al. [17] observed that spherical indentation is more sensitive to stress effects than sharp indentation. Thence, they proposed two methods of determining biaxial residual stress using spherical indentation. One is based on the fact that the contact pressure at the onset of yielding is affected by the residual stress, which can be analysed by Hertz contact mechanics, and then the biaxial stress can be determined via a closed form analytical solution. The other is based on the empirical observation that the curves representing the mean contact pressure versus normalized contact radius are vertically shifted as compared to the unstressed material by an amount very close to the magnitude of the residual stress.

In spite of the seemingly extensive literature on how to incorporate residual stress by using indentation, there are several shortcomings in these methods. They either require measuring the indentation area accurately, or only can be used to particular materials, e.g., perfectly elastic–plastic materials. In addition, some assumptions of the model result in large errors in the residual stress measurement.

Due to the complexity of the contact problem as well as high nonlinearity of materials involved in indentation, closed form solutions for the indentation curve are not readily available. Based on the FEM, the polynomial function of indentation was established by using the dimensional analysis method, but it is highly dependent on the precision of the curve or the surface fitting procedure. Artificial neural networks (ANNs) are universal approximations, which have been mathematically proved to be able to approximate any continuous non-linear function arbitrarily well as long as they contain at least one hidden layer. Models of ANN have been successfully constructed to solve many engineering problems. As ANNs do not require a complicated mathematical model, they have been widely applied to solve some complicated problems of indentation. Several researchers [18–23] adopted ANNs to characterize material properties using instrumented indentation.

In this paper, the shape of the load–depth curve is analysed. Based on the energy method and the dimensional analysis method, the database relationship

between the energy of residual stress, residual stress, and material properties is constructed. Reverse analysis using the ANN approach to characterize the mechanical properties is established from the finite element simulation results of spherical indentations on elastic–plastic strain-hardening materials. The residual stress and material properties can be extracted from indentation curves using the ANN approach.

2. THEORETICAL ANALYSIS

In an indentation test, an indenter is pressed into the specimen's surface to reach a preset maximum depth or a preset maximum force, and then the indenter is removed. During this procedure, it is assumed that the indented surface is subjected to an equi-biaxial in-plane residual stress and that the residual stress is uniform over the depth of the indentation. In addition, assuming the unloading process is unaffected by the residual stress, the indentation has an elastic–plastic loading and elastic unloading response.

Several studies have found that the shape of the loading and the unloading curves of the stressed sample deviates from the ideal shape of the unstressed sample [8,10,14], as shown in Fig. 1. A stressed sample subjected to indentation, if compared to an unstressed one, is naturally expected to exhibit a different mechanical response in terms of the indentation curve and imprint geometry. If the initial state of the residual stress is predominantly tensile, the material generally starts yielding at a larger depth applied to the indenter for a given indentation load, as compared to the case of an unstressed specimen; vice versa, if it is compressive. In other words, for a given indentation depth, the residual

compressive stress tends to increase the curvature and the maximum penetration load will be larger (Fig. 1, curve OCD), whereas a residual tensile stress reduces the curvature and results in a lower indentation force (Fig. 1, curve OEF). Also the amount of material sink-in/pile-up at the contact boundary turns out to be very sensitive to the presence of initial stress [24,25]: namely, sink-in increases when the material is subjected to tensile stress and pile-up increases in the compressive stress case.

Consider the case of a different residual stress. If the residual depth is the same as that of the unstressed sample, it should increase the indentation depth for the residual compressive stress, or decrease the indentation depth for the residual tensile stress. However, in case of residual compressive stress, it should extend the curve OC and BA in Fig. 1 through to intersect at point G. That is, if the indentation depth is h_{t1} when the sample is subjected to the residual compressive stress, after complete unloading the residual depth will be h_{r0}. Similarly, for the case of residual tensile stress, the loading curve OE intersects the curve AB at the point H. That is, when the indentation depth is h_{t2} if the initial state of self-stress is tensile, then the residual depth will be h_{r0} after complete unloading.

During loading, the area enclosed by the loading curves represents the indentation load energy, e.g. the area of OAN. When completing unloading, the area enclosed by the unloading curves represents the elastic recoverable energy, e.g. the area of BAN. When the specimen is free of stress, the net area enclosed by the loading and unloading curves represents the energy lost in plastic deformation, e.g. the area of OAB.

We will assume equivalence in the plastic energy for indents when the residual depth is the same. Thus, when the indentation depth is h_{t1} with the residual compressive stress or h_{t2} with the residual tensile stress, their plastic energy is the same as that of the indentation depth h_{t0} with free stress because they have the same residual indentation depth h_{r0}. In other words, the plastic energies of all of them are in the area of OAB in all cases the residual depth is h_{r0}. Because the area of OGAB or OHB as shown in Fig. 1 is the sum of the energy in plastic deformation and the energy contribution of the residual stresses, the area of OGA or OAH is the energy contribution of the residual stresses W_r.

Dimensional analysis has been successfully used to analyse indentation response. Based on dimensional analysis and FEM, Cheng and Cheng [26] presented several scaling relationships that provide a new insight into the shape of indentation curves.

For the spherical indentation of elastic–plastic material, during the loading procedure the indentation load F must be a function f_L of the following nine independent parameters: Young's modulus E, Poisson's ratio ν of the elastic–plastic solid, Young's
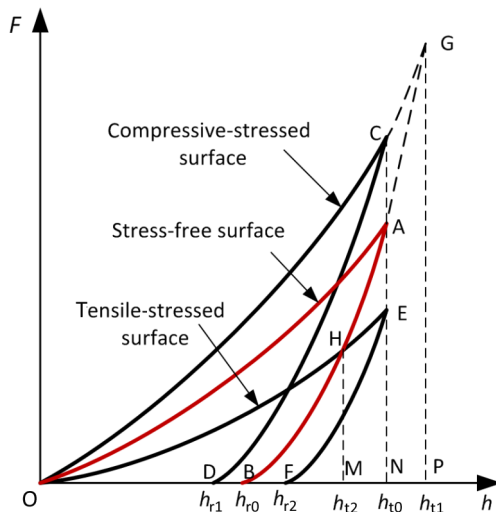

Fig. 1. Indentation load–depth curves for specimens with and without residual stress.

modulus E_i, Poisson's ratio ν_i of the elastic indenter, the yield strength σ_y, the strain-hardening exponent n, the residual stress σ_r, the indentation depth h, and the indenter radius R, i.e.:

$$F = f_L(E, \nu, E_i, \nu_i, \sigma_y, \sigma_r, n, h, R). \tag{1}$$

Using the reduced Young's modulus:

$$\frac{1}{E^*} = \frac{1-\nu^2}{E} + \frac{1-\nu_i^2}{E_i}. \tag{2}$$

Equation (1) can be reduced to

$$F = f_L(E^*, \sigma_y, \sigma_r, n, h, R). \tag{3}$$

By applying the Π theorem in dimensional analysis, Eq. (3) can be expressed as

$$\frac{F}{\sigma_y h^2} = \Pi_\alpha\left(\frac{E^*}{\sigma_y}, \frac{\sigma_r}{\sigma_y}, n, \frac{R}{h}\right), \tag{4}$$

where the dimensionless function Π_α relates the indentation response to the mechanical properties and indentation parameters.

The work done by indentation is

$$W_t = \int_0^{h_t} F dh = \int_0^{h_t} \sigma_y h^2 \Pi_\alpha dh = \sigma_y h_t^3 \Pi_\beta\left(\frac{E^*}{\sigma_y}, \frac{\sigma_r}{\sigma_y}, n\right). \tag{5}$$

Because unloading takes place after loading when the indenter reaches the maximum indentation depth h_t, the indentation unloading load F_u is a function f_u of ten independent parameters:

$$F_u = f_u(E, \nu, E_i, \nu_i, \sigma_y, \sigma_r, n, h, h_t, R). \tag{6}$$

Similarly, F_u can be expressed as:

$$F_u = \sigma_y h_t^2 \Pi_\gamma\left(\frac{E^*}{\sigma_y}, \frac{\sigma_r}{\sigma_y}, n, \frac{h}{h_t}, \frac{R}{h_t}\right). \tag{7}$$

The work done by material recovery is

$$W_u = \int_{h_r}^{h_t} F_u dh = \int_{h_r}^{h_t} \sigma_y h^2 \Pi_\gamma dh = \sigma_y h_t^3 \Pi_\varphi\left(\frac{E^*}{\sigma_y}, \frac{\sigma_r}{\sigma_y}, n\right). \tag{8}$$

Based on Eqs (5) and (8), the work done by residual stress and plastic deformation is

$$W_p = W_t - W_u = \sigma_y h_t^3 \Pi_\psi\left(\frac{E^*}{\sigma_y}, \frac{\sigma_r}{\sigma_y}, n\right). \tag{9}$$

Thus, in two different indentation depths, e.g. h_{t1} and h_{t0}, the ratio of the work done by residual stress to the work done by indentation load is

$$\frac{W_{r1}}{W_{t1}} = \frac{W_{p1} - W_{p0}}{W_{t1}} = \frac{h_{t1}^3 \Pi_{\psi1}\left(\frac{E^*}{\sigma_y}, \frac{\sigma_r}{\sigma_y}, n\right) - h_{t0}^3 \Pi_{\psi0}\left(\frac{E^*}{\sigma_y}, n\right)}{h_{t1}^3 \Pi_{\beta1}\left(\frac{E^*}{\sigma_y}, \frac{\sigma_r}{\sigma_y}, n\right)}$$

$$= \Pi_\chi\left(\frac{E^*}{\sigma_y}, \frac{\sigma_r}{\sigma_y}, n\right). \tag{10}$$

Combining Eqs (5), (8), (9), and (10) leads to

$$\frac{W_{u1}}{W_{t1}} = \Pi_1\left(\frac{E^*}{\sigma_y}, \frac{\sigma_r}{\sigma_y}, n\right), \tag{11}$$

$$\frac{W_{r1}}{W_{t1}} = \Pi_2\left(\frac{E^*}{\sigma_y}, \frac{\sigma_r}{\sigma_y}, n\right). \tag{12}$$

Thus, the two universal dimensionless functions, Π_1 and Π_2, can be used to relate the indentation response to the mechanical properties.

3. FINITE ELEMENT SIMULATION

In this work, elastic–plastic indentation was simulated by using the ABAQUS software on HP workstations [27]. The indenter was modelled as a sphere with a radius of 0.794 mm, and the specimen was treated as a body of revolution. The mesh used to model the specimen is shown in Fig. 2. The boundary conditions were defined as the roller boundary along the axis of symmetry, while the bottom boundary condition can also be defined as a roller boundary. The model was comprised of 19200 CAX3 mesh near the contact region and 4400 CAX4R mesh further away from the contact region to ensure numerical accuracy. At the maximum load, the minimum number of contact elements in the contact zone was no less than 25 in each FEM com-
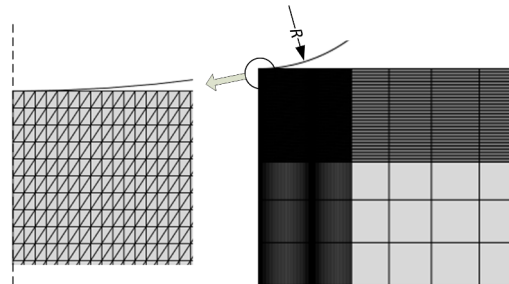

Fig. 2. The finite element mesh.

putation. The mesh was well tested for convergence and was determined to be insensitive to far-field boundary conditions. In all finite element computations, the indenter was modelled as a rigid body; the value of the friction coefficient between metallic surfaces and diamond is in the range of 0.10 to 0.15 as reported by Tabor [28]. A common constant value of 0.15 for friction between the diamond indenter and metallic materials was used throughout this study; and large deformation FEM computation was performed. The equi-biaxial compressive or tensile stress was added to the model by prescribing an initial stress in the finite element model. All simulations were performed in two different load–unload indentation cycles, the indentation depth was 30 μm and 50 μm, respectively.

The indented material was modelled as a homogeneous elastic–plastic von Misses solid with isotropic hardening. True stress and true strain are related via the following equation:

$$\sigma = E\varepsilon, \quad \varepsilon \geq \sigma_y/E.$$
$$\sigma = \sigma_y(E/\sigma_y)^n \varepsilon^n, \quad \varepsilon \geq \sigma_y/E. \tag{13}$$

To cover a wide variety of elastic–plastic materials, Young's modulus $E = 10, 50, 90, 130, 170, 210$ GPa and yield strength $\sigma_y = 200, 300, 500, 700, 1000, 1800, 2100, 3000$ MPa were used. The values of E/σ_y were varied over the range $100 \leq E/\sigma_y \leq 1000$, which covers most metals. Poisson's ratio is not an important factor in the indentation experiment [26], and for most engineering materials $\nu \approx 0.3$. The strain-hardening exponent was varied from 0 to 0.5; for most metals n is between 0.1 and 0.5.

The load–depth curve of the indentation was obtained by recording the reaction forces on the indenter and the corresponding applied displacements. The focus of this study was the indentation load–depth behaviour; there-

fore analysis of load–depth curves was used in indentation techniques to provide a measurement of the work. So the proper parameters were set in solution controls of ABAQUS to ensure the steps of loading and unloading were greater than 20.

In this study, both loaded and unloaded indentations were studied to establish how the response of spherical indentation was influenced by the residual stress and material properties. Residual indentation depth h_r and maximum load F_m were obtained from the load–depth curves for each given h_t. The total work W_t and reversible work W_u were obtained by integrating the loading and unloading curves, respectively.

The dimensionless function can be numerically derived from extensive finite element simulations. The surfaces denoted by the functions Π_1 and Π_2 are shown in Fig. 3 and Fig. 4. They illustrate the variations of W_u/W_t and W_r/W_t with respect to E^*/σ_y, σ_r/σ_y, and n for different indentation depths. It can be seen from Fig. 3a and Fig. 4a that W_u/W_t increases with n, but W_u/W_t decreases with increasing E^*/σ_y (or σ_r/σ_y). It is easy to understand that when E^*/σ_y (or σ_r/σ_y) increases or n decreases, the material is softer, so the elastic recovery of the material is smaller. As the indentation depth increases, the work done by loading increases faster than the work done by unloading. So W_u/W_t decreases with increasing indentation depth. From Fig. 3b and Fig. 4b we can see that the effects on W_r/W_t of compressive stress are often not as large as tensile stress, especially in the case of smaller E^*/σ_y. When E^*/σ_y is smaller, the effects on W_r/W_t of n are larger in the case of tensile stress. Figures 3b and 4b are similar because the change in the amount of W_r and W_t is approximate in the case of 30 μm and 50 μm.

If we obtain the function relationship of W_u/W_t or W_r/W_t, and E^*/σ_y, σ_r/σ_y, n, respectively, then E^*/σ_y, σ_r/σ_y, and n can be determined. It can be
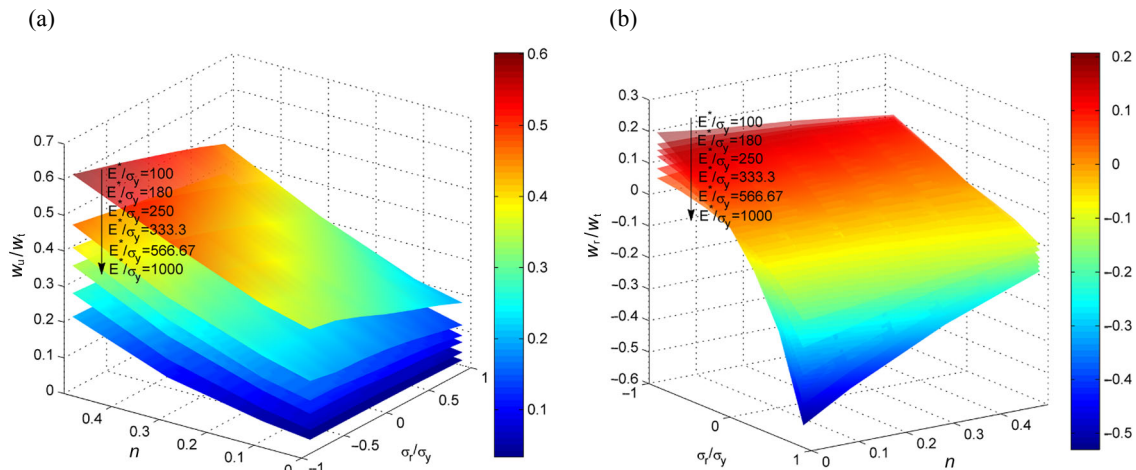

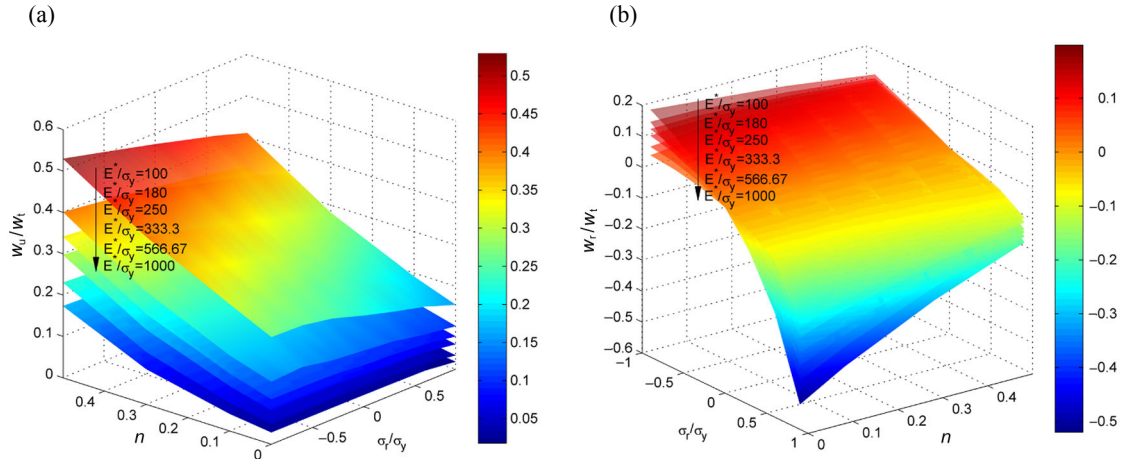**Fig. 3.** Variation of (a) W_u/W_t and (b) W_r/W_t based on the indentation depth of 30 μm.

Fig. 4. Variation of (a) W_u/W_t and (b) W_r/W_t based on the indentation depth of 50 μm.

seen from Fig. 3 and Fig. 4 that the relationship between W_u/W_t or W_r/W_t and E^*/σ_y, σ_r/σ_y, and n is a non-linear function. Due to the complexity of the functions, it is difficult to get an analytic function to describe their relationship; a trial and error procedure is normally necessary. Moreover, the accuracy of such an approach is highly dependent on the precision of the surface fitting procedure as well as the robustness of the reverse analysis algorithm.

4. ARTIFICIAL NEURAL NETWORKS

The flowchart in Fig. 5 outlines the process of determining the residual stress and material properties by using

Fig. 5. Flowchart for ANN.

ANNs. Finite element simulations are used to obtain the relationship between the dimensionless functions and the residual stress and material parameters. To fully train/test the ANNs, the dimensionless functions are networks' inputs and the residual stress and material parameters are networks' output. The inputs to ANN P_i are

$$P_i = \begin{pmatrix} W_{u(h003)}/W_{t(h003)} \\ W_{r(h003)}/W_{t(h003)} \\ W_{u(h005)}/W_{t(h005)} \\ W_{r(h005)}/W_{t(h005)} \end{pmatrix}, \quad (14)$$

where the subscripts $h003$ and $h005$ represent the indentation depths of 30 μm and 50 μm, respectively.

The outputs from the network T_i are

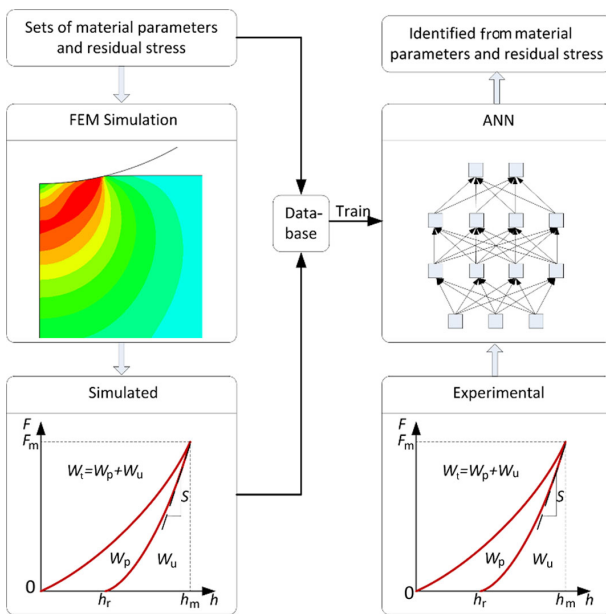$$T_i = \begin{pmatrix} E^*/\sigma_y \\ \sigma_r/\sigma_y \\ n \end{pmatrix}. \quad (15)$$

Back-propagation multilayer feed-forward ANN is created by using the Neural Network Toolbox in Matlab [29]. It comprises the input layer, the hidden layer, and the output layer. The number of neurons in the input and output layers of the ANN is identical to the number of input and output parameters, respectively. However, the number of neurons in the hidden layers of the neural network is calibrated during the training and validation process. The tangent sigmoid transfer function is used in the ANN.

The surfaces described by functions Π_1 and Π_2 as shown in Fig. 3 and Fig. 4 are used to serve as the training and validating data sets for ANN models. Training is the process of repeated applications of the back-propagation algorithm until the error becomes acceptable or some other criterion is achieved. Since the difference between the training data is larger, this will result in a

larger ANN prediction error. Thus, it is necessary to normalize the experiment data before applying them to the network. The normalizing equation is

$$x_k = \frac{x - x_{min}}{x_{max} - x_{min}}, \qquad (16)$$

where x is the real value of the variable before normalization, x_{min} and x_{max} are the minimum and maximum values of the variable x. They are normalized to the values x_k.

The training algorithm of gradient descent with momentum is used in our study to train the ANNs. The data for training and validation of ANN were obtained numerically through 280 finite element simulations. Out of the 280 sets of input and output data, 240 sets were randomly assigned as training data while the remaining 40 sets were used for validation purposes. The mean square error (MSE) of the network outputs and the target values are used as the network performance indicator. During training, the learning rule is used to iteratively adjust the weights and biases of the network in order to move the network outputs closer to the target values by minimizing the network performance indicator. In an effort to more properly reflect inter-mediate values of indentation, the numbers of neurons in three hidden layers are 200, 100 and 10.

5. RESULTS AND DISCUSSION

After the ANNs are successfully trained and tested, the ANN model maps the functional relationship between the dimensionless function and the mechanical para-meters. In order to examine the accuracy of the ANN

approach, several numerical experiments of indentation were performed. The results of testing conducted on 35 experimental data sets are presented in Fig. 6. It should be noted that these sets of finite element results were not used in the training and validation process described in Section 4.

It can be observed from Fig. 6 that the proposed ANN model predicted the residual stress and material properties reasonably accurately. The maximum error is less than 9% between the original input data and reverse analysis for all examined σ_r/σ_y, less than 13% for n, and less than 4% for E^*/σ_y.

There are potentially many sources of errors in physical experiments, which result in calculation errors of the residual stress and material properties. Therefore, we will investigate the sensitivity of this method for errors in the measured parameters such as W_u and W_r.

First, W_u of the indentation depth of 30 μm is given 2% error, while the other parameters are unchanged. The proposed ANN model is conducted to obtain the residual stress and material properties. The results are summarized in Fig. 7a. The maximum error is larger than 30% for σ_r/σ_y, 25% for n, and 46% for E^*/σ_y. Similarly analysis of W_r is examined. Comparing the input data with those identified from ANN in Fig. 7b, we can find that most reverse analysis results are fairly accurate of strain-hardening exponent and σ_r/σ_y. However, the error of E^*/σ_y is larger. This means that E^*/σ_y obtained from ANN algorithm are more sensitive to the measured parameters errors compared to σ_r/σ_y and n. Comparing Fig. 7a and Fig. 7b, we can find that the sensitivity for the error of W_u is larger than the error of W_r. This is because the relevance of W_r and σ_r is enhanced, so the error of W_r has reduced the impact on E^*/σ_y and n.
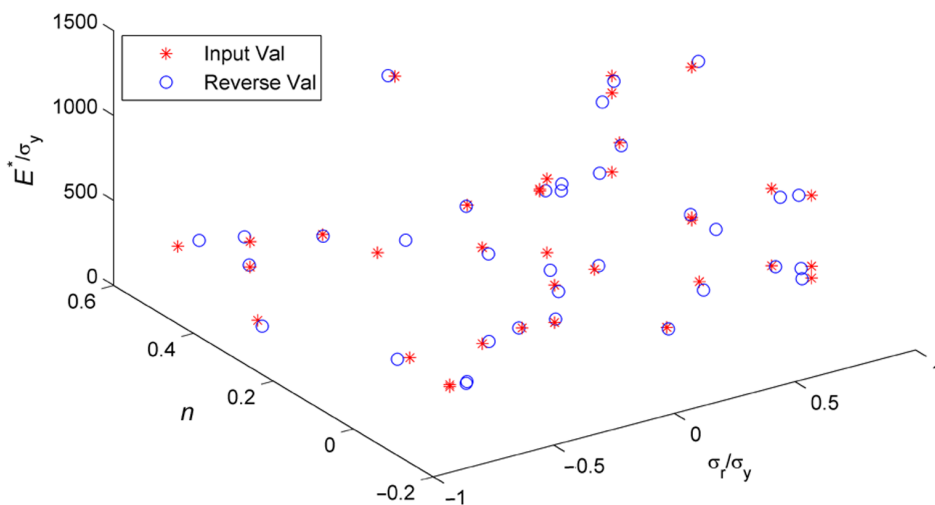

Fig. 6. Identification of E^*/σ_y, σ_r/σ_y, and n for ANN.

Fig. 7. Sensitivity of E^*/σ_y, σ_r/σ_y, and n for ANN: (a) W_u, (b) W_r.

6. CONCLUSIONS

An energy-based method and dimensional analysis of indentation parameters were applied to construct an artificial neural network model in order to extract the residual stress and material properties based on spherical indentation. The relationships between the work of residual stress, the residual stress, and material properties were numerically calibrated through training and validation of the ANN model. They enable the direct mapping of the characteristics of the indentation parameters to the residual stress and the elastic–plastic material properties. The proposed ANN can quickly and effectively predict the residual stress and material properties based on the load–depth curve of spherical indentation. It was found that E^*/σ_y obtained from the ANN algorithm was more sensitive to the errors of the measured parameters compared to σ_r/σ_y and n.

REFERENCES

1. Lu, J. *Handbook of Measurement of Residual Stresses*. The Fairmont Press, Lilburn, 1996.
2. Pethica, J. B., Hutchings, R., and Oliver, W. C. Hardness measurement at penetration depths as small as 20 nm. *Philos. Mag. A*, 1983, **48**, 593–606.
3. Oliver, W. C. and Pharr, G. M. An improved technique for determining hardness and elastic modulus using load and displacement sensing indentation experiments. *J. Mater. Res.*, 1992, **7**, 1564–1583.
4. Tunvisut, K., Busso, E. P., O'dowd, N. P., and Brantner, H. P. Determination of the mechanical properties of metallic thin films and substrates from indentation tests. *Philos. Mag. A*, 2002, **82**, 2013–2029.
5. Luo, J., Lin, J., and Dean, T. A. A study on the determination of mechanical properties of a power law material by its indentation force-depth curve. *Philos. Mag.*, 2006, **86**, 2881–2905.
6. Fernandes, J. V., Antunes, J. M., Sakharova, N. A., Oliveira, M. C., and Menezes, L. F. Young's modulus of thin films using depth-sensing indentation. *Phil. Mag. Lett.*, 2010, **90**, 9–22.
7. Khan, M. K., Hainsworth, S. V. Fitzpatrick, M. E., and Edwards, L. A combined experimental and finite element approach for determining mechanical properties of aluminium alloys by nanoindentation. *Comp. Mater. Sci.*, 2010, **49**, 751–760.
8. Suresh, S. and Giannakopoulos, A. E. A new method for estimating residual stresses by instrumented sharp indentation. *Acta Mater.*, 1998, **46**, 5755–5767.
9. LaFontaine, W. R., Paszkiet, C. A., Korhonen, M. A., and Li, C. Y. Residual stress measurements of thin aluminum metallizations by continuous indentation and x-ray stress. *J. Mater. Res.*, 1991, **6**, 2084–2090.
10. Lee, Y. H. and Kwon, D. Residual stress in DLC/Si and Cu/Si systems: application of a stress-relaxation model to the nanoindentation technique. *J. Mater. Res.*, 2002, **17**, 901–906.
11. Chen, X., Yan, J., and Karlsson, A. M. On the determination of residual stress and mechanical properties by indentation. *Mater. Sci. Eng. A*, 2006, **416**, 139–149.
12. Zhao, M. H., Chen, X., Yan, J., and Karlsson, A. M. Determination of uniaxial residual stress and mechanical properties by instrumented indentation. *Acta Mater.*, 2006, **54**, 2823–2832.
13. Yan, J., Chen, X., and Karlsson, A. M. Determining equibiaxial residual stress and mechanical properties from the force-displacement curves of conical microindentation. *J. Eng. Mater. Technol.*, 2007, **129**, 200–206.
14. Xu, Z. H. and Li, X. Estimation of residual stresses from elastic recovery of nanoindentation. *Philos. Mag.*, 2006, **86**, 2835–2846.

15. Wang, Q., Ozaki, K., Ishikawa, H., Nakano, S., and Ogiso, H. Indentation method to measure the residual stress induced by ion implantation. *Nucl. Instrum. Methods B*, 2006, **242**, 88–92.
16. Dean, J., Aldrich-Smith, G., and Clyne, T. W. Use of nanoindentation to measure residual stresses in surface layers. *Acta Mater.*, 2011, **59**, 2749–2761.
17. Swadener, J. G., Taljat, B., and Pharr, G. M. Measurement of residual stress by load and depth sensing indentation with spherical indenters. *J. Mater. Res.*, 2001, **16**, 2091–2102.
18. Skinner, A. J. and Broughton, J. Q. Neural networks in computational materials science: training algorithms. *Model. Simul. Mater. Sc.*, 1995, **3**, 371–390.
19. Huber, N. and Tsakmakis, C. Determination of constitutive properties from spherical indentation data using neural networks. Part I: The case of pure kinematic hardening in plasticity laws. *J. Mech. Phys. Solid*, 1999, **47**, 1569–1588.
20. Huber, N. and Tsakmakis, C. Determination of constitutive properties from spherical indentation data using neural networks. Part II: Plasticity with nonlinear isotropic and kinematic hardening. *J. Mech. Phys. Solid*, 1999, **47**, 1589–1607.
21. Tho, K. K., Swaddiwudhipong, S., Liu, Z. S., and Hua, J. Artificial neural network model for material characterization by indentation. *Model. Simul. Mater. Sc.*, 2004, **12**, 1055–1062.
22. Swaddiwudhipong, S., Tho, K. K., Liu, Z. S., Hua, J., and Ooi, N. S. B. Material characterization via least squares support vector machines. *Model. Simul. Mater. Sc.*, 2005, **13**, 993–1004.
23. Haj-Ali, R., Hoan-Kee, K., Sau, W. K., Saxena, A., and Rao, T. Nonlinear constitutive models from nanoindentation tests using artificial neural networks. *Int. J. Plast.*, 2008, **24**, 371–396.
24. Bolshakov, A., Oliver, W. C., and Pharr, G. M. Influences of stress on the measurement of mechanical properties using nanoindentation: Part II. Finite element simulations. *J. Mater. Res.*, 1996, **11**, 760–768.
25. Tsui, T. Y. and Pharr, G. M. Substrate effects on nanoindentation mechanical property measurements of soft films on hard substrates. *J. Mater. Res.*, 1999, **14**, 292–301.
26. Cheng, Y. T. and Cheng, C. M. Scaling relationships in conical indentation of elastic perfectly plastic solids. *Int. J. Solids Struct.*, 1999, **36**, 1231–1243.
27. *Abaqus Analysis Users Manual: Version 6.8*. Simulia, 2008.
28. Tabor, D. *The Hardness of Metals*. Clarendon Press, Oxford, 1951.
29. Matlab 2010. *Matlab 2010a*. The MathWorks Incorporate.

Energia-baasil-meetodiga jääkpingete ja materjalide omaduste määramine tehisneurovõrke kasutades

Hongping Jin, Wenyu Yang ja Lin Yan

On kasutatud energia- ja mõõtmelise analüüsi meetodite abil konstrueeritud tehisneurovõrkude mudeleid jääkpingete ning materjalide elastsete ja plastsete omaduste määramiseks sfäärilise indentori sissepressimise teel. Materjalides tekkivate jääkpingete ja materjalide omaduste ennustamine on indenteerimiskõverate abil teljestikus jõud-indenteerimissügavus kiirelt ning lihtsalt teostatav. Pakutud tehisneurovõrkude mudeli kalibreerimise protseduur võimaldab erinevate materjalide omaduste, nagu ühtlane võrdkaheteljeline jääkpinge, elastsusmoodul, voolepiir ja kalestumistegur, otse kaardistamist. Eelmainitud tehisneurovõrkude mudel on võrdlemisi täpne ja usaldusväärne.